# Revised structural phase diagram of $(Ba_{0.7}Ca_{0.3}TiO_3)$-$(BaZr_{0.2}Ti_{0.8}O_3)$

**Dean S. Keeble,[a] Feres Benabdallah,[b] Pam A. Thomas,[a] Mario Maglione[b] and Jens Kreisel.[a,c]**

a. Department of Physics, University of Warwick, Coventry CV4 7AL (UK).

b. ICMCB, Université de Bordeaux, CNRS,33600 Pessac (France)

c. Department Science and Analysis of Materials, CRP Gabriel Lippmann, Belvaux (Luxembourg)

The temperature-composition phase diagram of barium calcium titanate zirconate, ($x(Ba_{0.7}Ca_{0.3}TiO_3)$ -(1-$x$)($BaZr_{0.2}Ti_{0.8}O_3$); BCTZ) has been reinvestigated using high-resolution synchrotron x-ray powder diffraction. Contrary to previous reports of an unusual rhombohedral-tetragonal phase transition in this system, we have observed an intermediate orthorhombic phase, isostructural to that present in the parent phase, $BaTiO_3$, and we identify the previously assigned T-R transition as a T-O transition. We also observe the O-R transition coalescing with the previously observed triple point, forming a phase convergence region. The implication of the orthorhombic phase in reconciling the exceptional piezoelectric properties with the surrounding phase diagram is discussed.

Lead oxide based ferroelectric materials such as lead zirconate titanate ($PbZr_{1-x}Ti_xO_3$, PZT) are the most widely used piezoelectrics, because of their excellent properties. The microstructural origin of the remarkable piezoelectric properties remained puzzling for several decades, it was quickly recognized however that the complex structural phase diagram was key. In particular, it has been recognized that piezoelectric properties are maximized close to the structural phase transition from rhombohedral (R) to tetragonal (T) phases, which exists in a limited range of chemical composition: the so called morphotropic phase boundary (MPB). [1] These R and T phases do not have a

crystallographic group–subgroup relationship, and thus no continuous transition between them is possible. A breakthrough in the understanding of the remarkable piezoelectric properties of PZT was achieved by showing that the strong piezoelectric properties of these solid solutions can be interpreted *via* a 'polarisation rotation' between the adjacent R- and T-phases through one (or more) intermediate monoclinic phases[2, 3]. Subsequent work on other lead-containing piezoelectrics such as PMN-PT or PZN-PT has further underlined the need for knowledge of structural phase diagrams for both the understanding of remarkable properties, and the design of new improved piezoelectrics (see reviews [4-7]).

In recent years, the environmental and health hazards of lead have been recognized, so that recycling and disposal of devices containing lead-based piezoelectric materials became of great concern. As a consequence, there is an increasing interest in the development of lead-free piezoelectric materials[8-13] with the main challenge to develop materials with an equivalent or even higher piezoelectric response than the lead-based materials. Within this context, recent reports[14] of a high piezoelectric coefficient $d_{33}$ of 620 pC/N in the lead-free solid solution $0.5(BaZr_{0.2}Ti_{0.8}O_3)$-$0.5(Ba_{0.7}Ca_{0.3}TiO_3)$—albeit in a small temperature range—have attracted a significant research interest, as this value exceeds even the $d_{33}$ of soft PZT. This result has motivated further investigations of the whole solid solution $x(Ba_{0.7}Ca_{0.3}TiO_3)$ -$(1-x)(BaZr_{0.2}Ti_{0.8}O_3)$ - abbreviated to BCTZ - on both ceramics and thin film samples (e.g. [15-20]). The first structural phase diagram of BCTZ has been reported[14] and the different phase sequences with increasing temperature can be summarized as follows: (i) $x \leq 0.32$: a single phase transition is observed from the low temperature R-phase to the high-temperature prototype cubic $Pm\bar{3}m$ structure (C), (ii) $0.32 < x < 0.8$ : presence of two phase transitions through a R-T-C phase sequence and (iii) $x > 0.8$: a single phase transition from a T-phase to the C-phase. In-between (i) and (ii) the phase diagram was proposed to pass through a triple point, where three first-order phase transitions (C-T, C-R, and T-R) coincide and where the highest permittivity is observed.[14] Comparing these sequences to literature studies on $BaTiO_3$-based solid

solutions such as $BaTi_{1-x}B_xO_3$ ($B$ = Zr, Ce, Hf) it appears that the suggested R-C phase sequence is common to highly doped BTO-based materials, while the R-T-C sequence is unusual.[8, 21]

The aim of this work is to re-investigate the structural phase diagram of BCTZ, motivated by both the known importance of the structural phase diagram for understanding piezoelectrics and the uncommon nature of the R-T-C phase sequence reported previously. We are specifically interested in investigating the R-T sequence and to verify the potential presence of 1) an intermediate orthorhombic O-phase as in $BaTiO_3$-based materials; 2) a bridging M-phase as in PZT; 3) long-range octahedral tilts, which might be introduced by the Ca-substitution, knowing that $CaTiO_3$ manifests strong tilt instabilities. Structural distortions of perovskites are often subtle and difficult to detect, so we have chosen to use high-resolution powder diffraction experiments at a synchrotron source with small temperature steps to investigate four chemical compositions around the triple point.

Polycrystalline BCTZx (with compositions 20%, 32%, 40% and 50%) were synthesised by a conventional solid state reaction technique. Raw materials with stoichiometric fractions of $BaCO_3$ (99.95%), $TiO_2$ (99.9%), $CaCO_3$ (99.5%), and $ZrO_2$ (99.99%) were mixed and ground by ball milling for 2 h with the addition of alcohol. After drying, the powder mixtures were calcined at 1350 °C for 15 h in an oxygen atmosphere. All compositions were checked using standard XRD, SEM and X-ray microprobe to ensure phase purity and appropriate chemical content.

Powder diffraction was performed on the high-resolution powder diffraction beamline ID31 at the European Synchrotron Radiation Facility, Grenoble, France. The sample was packed into a 0.4mm diameter capillary, and spun at a rate of 20 Hz to remove preferred orientation effects. Photons of wavelength 0.35419(1) Å (E = 35.005(3) keV) were used and the diffracted intensities were collected using a multianalyser detector bank[22]. Rietveld refinements of the collected patterns were performed using Topas Academic[23].

The ceramics used for the dielectric measurements were made from the same powders used for the above X-ray investigation. The sintered pellets had relative density above 92%, diameter of 8mm and thickness of 1mm. The major faces were gold-electroded and set in a homemade temperature cell under a dry helium atmosphere: this is critical to avoid moisture condensation on the samples and the formation of ice on cycling through the ice point.

Before powder patterns suitable for Rietveld refinement were taken, a "snapshot" of the thermal variation of the whole pattern was collected. This procedure took advantage of the ability of the beamline apparatus to collect a sizeable pattern (~16° $2\theta$, comparable information content to a 100° $2\theta$ pattern using CuKα radiation) in seconds. Patterns were collected continuously whilst the temperature was ramped from 80 to 450 K, with each pattern covering around 2 K. When visualised as suitably-cropped contour plots, these collections yield an overview of the thermal development of the structure. This plot for BCTZ50 is shown in Figure 1 where a total of three phase transitions are observed in the temperature range studied. Furthermore, from the splitting of the peaks we can suggest crystal systems for the four phases present. *Phase A:* In the high temperature phase, denoted A in Figure 1, all of the pseudo-cubic peaks are singlets, strongly suggesting cubic symmetry. *Phase B*: the splitting of the $(100)_{pc}$ into a doublet and the continuation of the $(111)_{pc}$ as a singlet suggests a pseudo-cubic tetragonal symmetry. *Phase C:* As the $(111)_{pc}$ is now split, and the $(100)_{pc}$ remains split, we can suggest that the lattice is no longer pseudo-cubic. Instead, the splitting of the peaks is consistent with an $\sqrt{2}a \times \sqrt{2}a \times a$ orthorhombic supercell. *Phase D*: The resingularization of the $(100)_{pc}$ peak infers a return to a pseudo-cubic $a \times a \times a$ unit cell, and the large splitting of the $(111)_{pc}$ peak suggests a rhombohedral crystal lattice. This phase transition sequence (Cubic-Tetragonal-Orthorhombic-Rhombohedral) is identical to that of the parent phase of the system, $BaTiO_3$.

This sequence, however, depends on the chemical compositions of BCTZ, as illustrated by comparison of the $(220)_{pc}$ peak in all four compositions as a function of temperature in Figure 2. It

can be seen that BCTZ40 presents a similar phase sequence to BCTZ50, while BCTZ20 and BCTZ32 undergo only one phase transition. The splitting of the pseudo-cubic Bragg peaks in these materials is consistent with the low temperature rhombohedral structure of BCTZ50 and—indeed $BaTiO_3$—suggesting a direct transformation from the high temperature cubic phase to the low temperature rhombohedral phase. We note that no extra reflections consistent with octahedral tilting are observed in any pattern in the current study. We therefore conclude that despite the introduction of the small $Ca^{2+}$ cation, no long-range octahedral tilts are introduced to the structure.

To confirm the succession of 3 phase transitions for compositions beyond BCTZ32, we reconsidered the published dielectric data for BCTZ32 and BCTZ50 (ref [16]) and we undertook further investigations of BCTZ20 and BCTZ40. In our earlier work[16] and other reports[14, 15], dielectric and elastic experiments did show the succession of 3 phase transitions for BCTZ50, while a single transition was observed for BCTZ32. Despite being of low amplitude, the third transition (assigned above as R-O) did also appear in the dielectric data of Liu and Ren[14] for BCTZ50, although it was not considered as such. Our previous pyroelectric experiments made this third transition in BCTZ50 unquestionable[16]: this is readily seen in Figure 3 where $\partial\varepsilon'/\partial T$ is plotted for the 4 compositions. This shows that the single transition at low content (BCTZ20 and BCTZ32) is separated from the succession of 3 transitions in the high composition range (BCTZ40 and BCTZ50) by a small region of phase space. Since the Gibbs phase rule prohibits a single four-phase invariant point in a pseudo-binary phase diagram, we refer to this non-point-like region as a *phase convergence region*. The temperatures at which the dielectric anomalies are recorded are also in full agreement with the above structural investigations.

Why the two intermediate phases (O+T) both disappear at very similar compositions (in the phase convergence region), both in the current BCTZ solid solution and in the binary BZT, is an interesting question. Since both phases exist due to competing A- and B-site polar instabilities, leading to a reduction of the number of $Ti^{4+}$ $(111)_{pc}$ displacements from 8 (cubic) to 4 to 2 to 1 (rhombohedral) as temperature is decreased[24], we suspect that the critical energy of these phases is very similar,

although at no point degenerate. The addition of other species into the BTO structure does not change the overriding nature of the $Ti^{4+}$ to displace in $(111)_{pc}$ directions, but it does interfere with the delicate balance of forces required to stabilise the intermediate tetragonal (4 sites) and orthorhombic (2 sites) phases.

In order to confirm the suggested phase sequences and to assign a space group to the individual phase, full Rietveld refinements were performed on powder patterns collected for significantly longer times. The space groups of the phases of $BaTiO_3$ were used as an initial basis for the refinements, and in all the phases, these space groups (or mixtures thereof near transitions) yielded good fits to the data. Since there was no evidence to suggest lower space-group symmetry (such as tilt peaks or unexplained splitting) these space groups were accepted as correct. In all phases of all compositions studied, anisotropic peak widths were observed and were accounted for in the model by applying the corrections of Stephens[25]. Rietveld refinements confirm that the phase sequence observed in BCTZ50 and BCTZ40 is identical to that observed in $BaTiO_3$: i.e. $Pm\bar{3}m \rightarrow P4mm \rightarrow Amm2 \rightarrow R3m$. An example of an orthorhombic refinement and indicative fits of BCTZ50 at all temperatures is shown in Figure 4 (ref. 26). As $x$ is decreased further from BCTZ40 to BCTZ32 and beyond, we observe that the two intermediate phases $P4mm$ and $Amm2$ are suppressed and the three transitions coalesce to form one "pinched" transition directly from the low temperature $R3m$ phase to the high temperature $Pm\bar{3}m$ phase. This "pinching" of the transition (and the introduction of relaxor behaviour beyond[27]) is also seen in other $BaTiO_3$ based solid-solutions, and in the $Ba(Ti,Zr)O_3$ system in particular. In this system, the pinching of the transitions is driven by the competing elastic fields[28] of the different sized titanium and zirconium cations, and occurs when Zr/(Ti + Zr) reaches ~0.15. (ref. [29]) In the current solid-solution we observe the pinching occurring between the BCTZ32 and BCTZ40 compositions, corresponding to $0.12 < Zr/(Ti + Zr) < 0.136$.

This is a small yet significant compositional difference, and so we can infer an effect of the Ca substitution on the phase sequence. Based solely on the idea that phase convergence region occurs

at a composition of Zr = 0.15 in BTZ, one would expect it to occur in BCTZ**25** (which equates to Zr = 0.15 as in BTZ). As we observe the phase convergence at a lower Zr content, we conclude that the Ca substitution destabilises the intermediate $BaTiO_3$ structures further. This is likely due to the underlying and competing tilt instabilities induced by CTO, so that less Zr doping is needed to destabilise them completely and induce the single R-C transition.

In summary, we have observed an orthorhombic phase in the BCTZ system, which now makes the phase sequence (from low to high temperature) R-O-T-C for higher BCTZ compositions (Figure 5(a)). This is identical, both in sequence and in space group symmetry, to that of the parent phase of the system, $BaTiO_3$. Overall, this is to be expected: the addition of zirconium to $BaTiO_3$ destabilises tetragonal and orthorhombic phases, forcing the rhombohedral phase up to the Curie point, whilst the addition of calcium stabilises the tetragonal phase down to low temperature[30]. Since the two ends of the BCTZ phase diagram reported here are $BaTi_{0.8}Zr_{0.2}O_3$ (BTZ20 ≡ BCTZ0) and $Ba_{0.7}Ca_{0.3}TiO_3$ (BCT30 ≡ BCTZ100), one can think of the BCTZ solid solution as a way of traversing from BCT to BTZ without having to go *via* BTO as an intermediate. In so doing, the rate of change of instability with composition (hereafter referred to as the "instability gradient") is increased, manufacturing a more vertical phase boundary, much like that observed in an MPB. To emphasise this effect, the three dimensional phase diagram (the BTO-BCT30-BTZ20 triangle vs. T) is shown in Figure 5(b): circumventing BTO in going from BCT30 to BTZ20 can clearly be seen to increase the instability gradient. This quasi-stable region, a direct consequence of the high instability gradient, increases the degrees of freedom available to the system, and corresponds to a strongly degenerate free energy landscape. This degeneracy could enhance the extreme piezoelectric coefficients in this composition range[15]. Given the small dielectric anomaly associated with this third transition, and the high instability gradient associated with the orthorhombic phase, it is understandable why its existence has been unobserved until now: particularly given that the previous transition sequence was assigned solely on the basis of dielectric data. In spite of its small dielectric anomaly, and small phase volume occupancy, we believe the orthorhombic phase key to the properties of the BCTZ system.

One may consult the ternary phase diagram and try to manufacture an even greater instability gradient, by altering the end members of the solid-solution. Increasing the Zr content further in the BTZ end-member actually drives $T_C$ at that end if the solid-solution down, reducing the instability gradient. However, the addition of more Ca to the BCT end-member could enhance the properties further: by using BCT40 the tetragonal phase is even more stabilised at that end of the phase diagram, and an even larger instability gradient could be observed around the phase convergence region.

***Acknowledgements***

We would like to thank A. Fitch for his help with the synchrotron data collection. JK acknowledges financial support during his sabbatical stay at Warwick University from the Institute of Advanced Study (IAS) Warwick and from the Région Rhône-Alpes (CMIRA grant). DSK thanks the Science City Research Alliance and the HEFCE Strategic Development Fund for financial support.

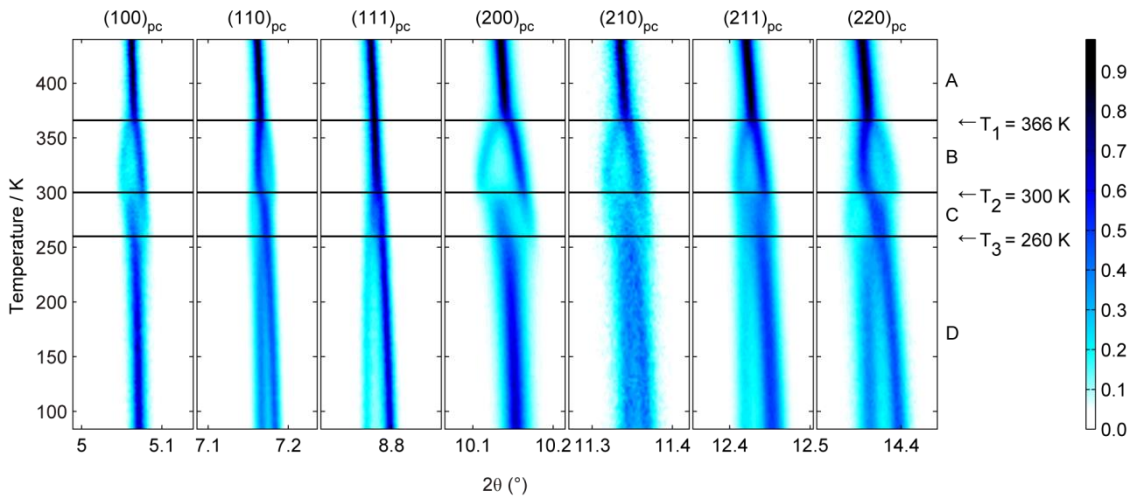


**Figure 1 - BCTZ50 "snapshot". Normalised contour maps showing the evolution of the first 7 pseudo-cubic peaks with temperature for BCTZ50. Three distinct phase transitions are observed (black lines), suggesting four distinct phases (A-D), identified from the peak splitting as cubic (A); tetragonal (B); orthorhombic (C); rhombohedral (D).**

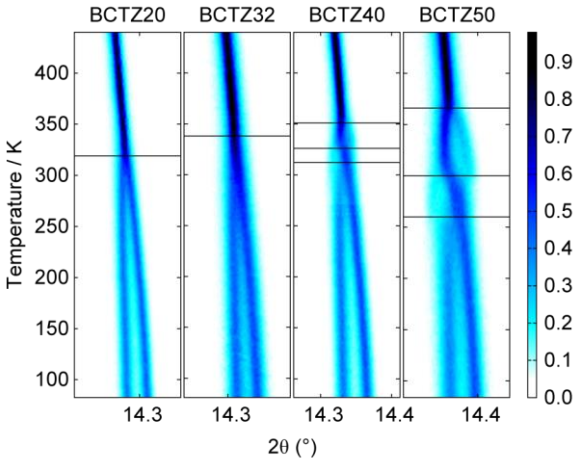


**Figure 2 - Comparison of the normalised $(220)_{pc}$ peak in the four compositions studied in the present work. The three phase transitions observed in BCTZ50 are "pinched" together as x is decreased, until in BCTZ32 (and below) only one transition remains. The temperature of this initial cubic-symmetry breaking transition also increases monotonically with x.**

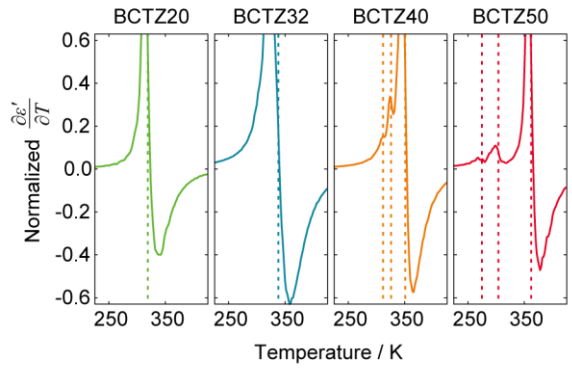


**Figure 3 - Derivative of the relative real part of the dielectric permittivity versus temperature for the BCTZ compositions under investigation. The operating frequency was 10 kHz. The lines indicate transitions, the temperatures of which correspond to the maxima in $-\partial^2\varepsilon' / \partial T^2$.**

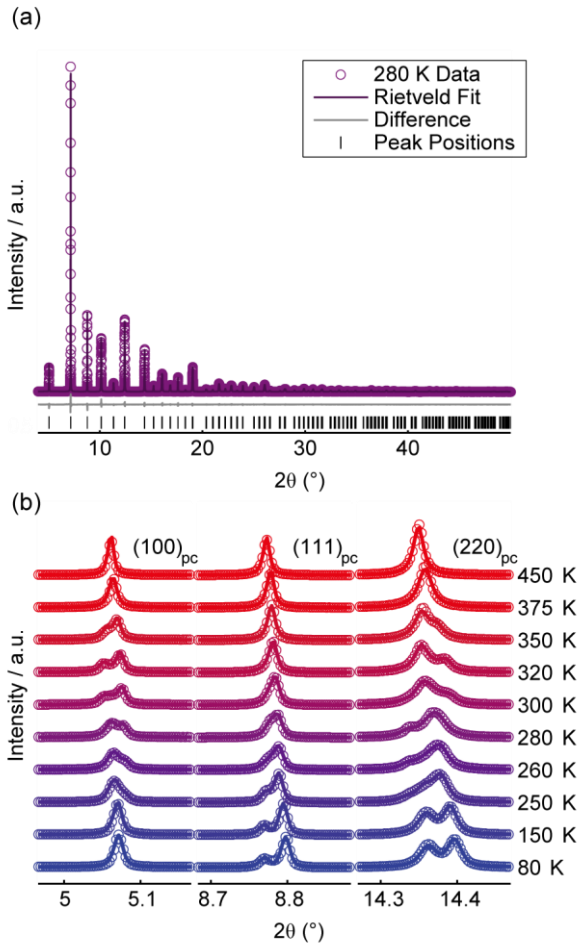


**Figure 4 – Rietveld refinements of BCTZ50. (a) Whole pattern refinement fit of the 280 K data using an orthorhombic $Amm2$ structure; (b) Variable temperature Rietveld fits for the $(100)_{pc}$, $(111)_{pc}$ (× 0.5), and $(220)_{pc}$ reflections in BCTZ50. The Rietveld fit (solid line) matches the as-collected data (open circles) well for all temperatures studied.**

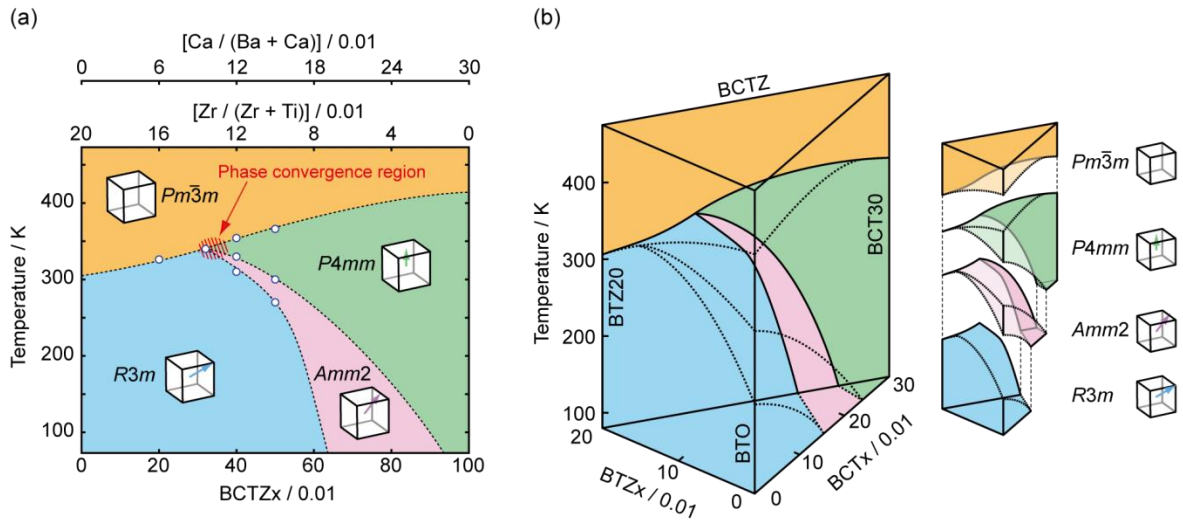


**Figure 5 – Phase diagrams of BTO solid-solutions (a) Suggested phase diagram of BCTZ based on the current study. In contrast to the previous work of Liu (see Ref 14), we observe the orthorhombic *Amm*2 phase persisting all the way to the phase convergence region. (b) 3D phase diagram of BCTZ, showing how the two binary BTZ and BCT phases combine to form the ternary BCTZ, including an exploded view emphasising the connectivity of the phases. This 3D representation highlights the formation of the high instability gradient: in traversing from the left edge (BTZ20) to the right edge (BCT30) via the parent phase BTO, the elimination of the Zr-induced pinching of the transitions and the introduction of the Ca-induced stabilisation of the tetragonal phase occur sequentially. However, in traversing from BTZ20 to BCT30 directly, these two effects occur simultaneously, manufacturing the larger instability gradient.**

References


1 M. E. Lines and A. M. Glass, *Principles and Applications of Ferroelectrics* (Clarendon Press, Oxford, 1977).

2 B. Noheda, D. E. Cox, G. Shirane, J. A. Gonzalo, L. E. Cross, and S. E. Park, Applied Physics Letters **74**, 2059 (1999).

3 B. Noheda, J. A. Gonzalo, L. E. Cross, R. Guo, S. E. Park, D. E. Cox, and G. Shirane, Physical Review B (Condensed Matter) **61**, 8687 (2000).

4 D. E. Cox, B. Noheda, G. Shirane, Y. Uesu, K. Fujishiro, and Y. Yamada, Applied Physics Letters **79**, 400 (2001).

5 B. Noheda, Current Opinion in Solid State & Materials Science **6**, 27 (2002).

6 B. Noheda and D. E. Cox, Phase Transitions **79**, 5 (2006).

7 M. Davis, Journal of Electroceramics **19**, 25 (2007).

8 J. Ravez and A. Simon, Journal of the Korean Physical Society **32**, S955 (1998).

[9] T. Takenaka and H. Nagata, Key Engineering Materials **157**, 57 (1999).
[10] M. D. Maede, D. Damjanovic, and N. Setter, J. Electroceram. **13**, 395 (2004).
[11] Y. Saito, H. Takao, T. Tani, K. Nonoyama, K. Takatori, T. Homma, T. Nagaya, and M. Nakamura, Nature **432**, 84 (2004).
[12] T. R. Shrout and S. J. Zhang, J. Electroceram. **19**, 113 (2007).
[13] J. Rodel, W. Jo, K. T. P. Seifert, E. M. Anton, T. Granzow, and D. Damjanovic, Journal of the American Ceramic Society **92**, 1153 (2009).
[14] W. Liu and X. Ren, Physical Review Letters **103**, 257602 (2009).
[15] D. Damjanovic, A. Biancoli, L. Batooli, A. Vahabzadeh, and J. Trodahl, Applied Physics Letters **100**, 192907 (2012).
[16] F. Benabdallah, A. Simon, H. Khemakhem, C. Elissalde, and M. Maglione, Journal of Applied Physics **109**, 124116 (2011).
[17] A. Piorra, A. Petraru, H. Kohlstedt, M. Wuttig, and E. Quandt, Journal of Applied Physics **109**, 104101 (2011).
[18] V. S. Puli, A. Kumar, D. B. Chrisey, M. Tomozawa, J. F. Scott, and R. S. Katiyar, Journal of Physics D: Applied Physics **44**, 395403 (2011).
[19] J. Gao, et al., Applied Physics Letters **99**, 092901 (2011).
[20] D. Xue, Y. Zhou, H. Bao, C. Zhou, J. Gao, and X. Ren, Journal of Applied Physics **109**, 054110 (2011).
[21] A. Simon, J. Ravez, and M. Maglione, Journal of Physics: Condensed Matter **16**, 963 (2004).
[22] J. L. Hodeau, P. Bordet, M. Anne, A. Prat, A. N. Fitch, E. Dooryhee, G. Vaughan, and A. Freund, in *Conference on Crystal amd Multilayer Optics*, San Diego, Ca, 1998).
[23] A. A. Coelho, (Coelho Software, 2007).
[24] B. Ravel, E. A. Stern, R. I. Vedrinskii, and V. Kraizman, Ferroelectrics **206**, 407 (1998).
[25] P. W. Stephens, Journal of Applied Crystallography **32**, 281 (1999).
[26] See supplementary material at (URL) for full Rietveld refinement fits of all compositions studied.
[27] A. R. Akbarzadeh, S. Prosandeev, E. J. Walter, A. Al-Barakaty, and L. Bellaiche, Physical Review Letters **108**, 5 (2012).
[28] C. Laulhe, A. Pasturel, F. Hippert, and J. Kreisel, Physical Review B **82** (2010).
[29] T. Maiti, R. Guo, and A. S. Bhalla, Journal of the American Ceramic Society **91** (2008).
[30] T. Mitsui and W. B. Westphal, Physical Review **124**, 1354 (1961).